

An Equation of State for Turbulence in the Gross-Pitaevskii model

Gevorg Martirosyan,^{1,*} Kazuya Fujimoto,² and Nir Navon^{3,4}

¹*Cavendish Laboratory, University of Cambridge, J. J. Thomson Avenue, Cambridge CB3 0HE, United Kingdom*

²*Department of Physics, Tokyo Institute of Technology,
2-12-1 Ookayama, Meguro-ku, Tokyo 152-8551, Japan*

³*Department of Physics, Yale University, New Haven, Connecticut 06520, USA*

⁴*Yale Quantum Institute, Yale University, New Haven, Connecticut 06520, USA*

(Dated: July 12, 2024)

We report the numerical observation of a far-from-equilibrium equation of state (EoS) in the Gross-Pitaevskii model. This universal dimensionless EoS is constructed by relating the turbulent cascade's scale-free spectrum amplitude to the energy flux of the steady state that emerges from the large-length-scale driving of a Bose-Einstein condensate (BEC). Remarkably, this EoS defies the generic predictions of wave-turbulent kinetic theory, even though the cascade spectra are quantitatively well understood within that theory. Finally, we find that the concept of quasi-static thermodynamic processes between equilibrium states extends to far-from-equilibrium steady states.

Equilibrium and near-equilibrium thermodynamics are conceptual cornerstones in physics, reducing the description of complex many-body systems of many degrees of freedom to relationships between a few macroscopic observables. When a system is in a far-from-equilibrium state, such a general framework does not exist, and unveiling universal features in such scenarios has been a major goal in modern physics. In situations where local equilibrium holds, the framework of local thermodynamics and hydrodynamics can provide a bridge to universal descriptions [1–3]. In the cases where even microscopic equilibrium is not realized, universal features have also been predicted theoretically and observed experimentally; some examples include the thermalization of states far from equilibrium [4–10] and the description of far-from-equilibrium steady states in terms of state variables that are linked by far-from-equilibrium analogs of equations of state (EoS) [11–13].

Remarkable examples of steady states that are even locally far from equilibrium are matter-wave turbulent cascades, sustained by energy injection and dissipation that occur on different length scales. Recently, these states have been cleanly realized in a cold-atomic setting [14, 15], and a far-from-equilibrium EoS was measured for the turbulent state [13]. The simplest approach to describe these experiments is the classical-field Gross-Pitaevskii (GP) equation. Although this model has been studied for decades (see *e.g.* [16, 17]) – and indeed its equilibrium and near-equilibrium properties are well established – it is notable that much of its far-from-equilibrium content remains to be understood [18]. A successful approach to understanding the GP description in a far-from-equilibrium setting is the perturbative framework of weak wave turbulence (WWT), which predicts the existence of a far-from-equilibrium EoS, the Kolmogorov-Zakharov spectrum [20–22]. However, this solution does not match the experimentally measured EoS [13], which motivates a non-perturbative study of wave-turbulent cascades in the GP model.

In this Letter, we show that the GP model possesses a far-from-equilibrium EoS that lies outside the paradigm of tradi-

tional wave-turbulence kinetics [23]. The turbulent state obtained at long times is steady and is characterized by a momentum distribution quantitatively described by a universal prediction from WWT. This steady state possesses the hallmarks of a direct energy cascade, *i.e.* that the dissipation-scale-independent energy flux is scale invariant, transporting energy from large to small length scales. However, the power-law scaling of the amplitude of the momentum distribution with the energy flux is starkly different from the predictions of wave-kinetics theory.

Our study is based on the universal GP model

$$i\hbar \frac{\partial \psi}{\partial t} = \left(-\frac{\hbar^2}{2m} \nabla^2 + g|\psi|^2 \right) \psi, \quad (1)$$

for the field $\psi(\mathbf{r}, t)$. This equation, also known as the non-linear Schrödinger equation, is a universal wave equation that describes a variety of systems, such as optical fields in non-linear Kerr media [24], weakly interacting Bose-Einstein condensates [25], and gravity waves in deep inviscid fluids [26]. We focus on the system of the weakly interacting Bose gas in 3D, where $\psi(\mathbf{r}, t)$ is interpreted as the classical field of the Bose gas, $g = 4\pi\hbar^2 a/m$ is the strength of the interatomic interactions, m is the atomic mass, and a is the s -wave scattering length. The field is normalized to $\int |\psi(\mathbf{r}, t)|^2 d^3\mathbf{r} = N$, where N is the (instantaneous) particle number.

Recent experimental studies have shown that this classical field model is relevant to describe a wave-turbulent scale-invariant steady state of a quantum degenerate Bose gas driven at large length scales and dissipated at small ones [14, 15]. To study far-from-equilibrium properties of the GP model Eq. (1), we add trapping, forcing, and dissipation terms in its right-hand side, of the form $V(\mathbf{r}, t) = V_{\text{box}}(\mathbf{r}) + V_{\text{drive}}(\mathbf{r}, t) + V_{\text{diss}}(\mathbf{r})$ (see [27]). The first contribution, V_{box} , is the confining potential that describes an atomic box trap [28]. For experimental relevance, we use a cylindrical potential (oriented along the z axis) of radius R and length L [see the cartoon of Fig. 1(a)] [29]. The second term is a forcing at the length scale of the system size, $V_{\text{drive}}(\mathbf{r}, t) = U_s \sin(\omega t)z/L$. The natural scale for the drive amplitude U_s is set by gn , where $n = N/V$

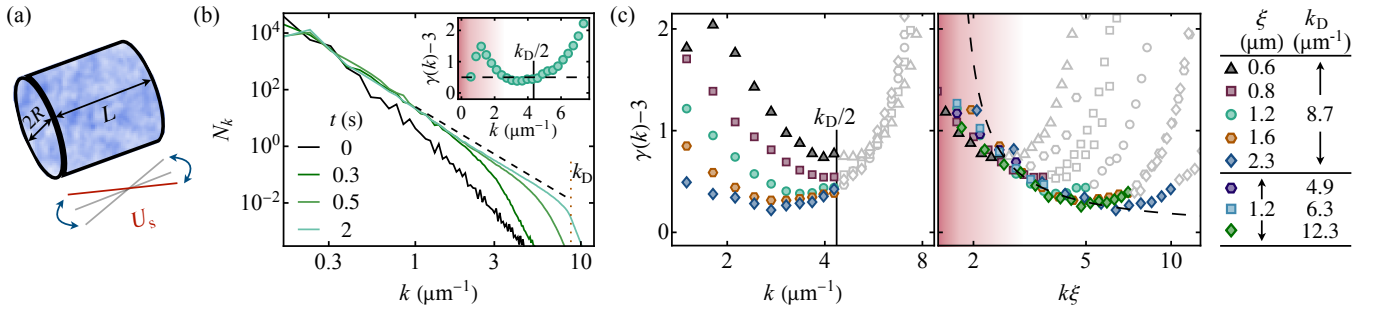


FIG. 1. The direct turbulent cascade in the GP model. (a) Cartoon of the simulation geometry and the driving protocol. We use a cylindrical box trapping potential of length L and radius R , and the energy is injected into the system by applying a time-periodic potential gradient $V_{\text{drive}}(\mathbf{r}, t) = U_s \sin(\omega t) z/L$ (see text for typical parameters). (b) The build-up of the turbulent cascade; the mode occupation number N_k is shown for various shaking times t . At long times, the system is in a steady state with $N_k \propto k^{-\gamma}$ (the dashed line corresponds to $\gamma = 3.5$). The inset shows the cascade exponent $\gamma(k) \equiv -d \ln[n(k)]/dk$, calculated from the continuous momentum distribution $n(k)$; the dashed line is $\gamma(k) = 3.5$. The red shading indicates the region of momentum space where the weak interaction approximation is not valid (see text). Here, the simulation parameters are $L = 50 \mu\text{m}$, $R = 15 \mu\text{m}$, $U_s = 1.0\zeta$, $\omega = 2\pi \times 10\text{Hz}$, and $a = 100a_0$ (corresponding to $\xi = 1.2 \mu\text{m}$ and $\tau = 10\text{ms}$). (c) The cascade exponent $\gamma(k)$ for different system parameters. (left) $\gamma(k)$ for different interactions is not universal, and it bends up around $k_D/2$ (solid line). (right) The rescaled data for γ versus $k\xi$ collapse in the range $2.5 \lesssim k\xi \lesssim k_D\xi/2$, demonstrating that the effective injection scale k_0 of the isotropic 4-wave cascade is $\propto k_\xi \equiv 1/\xi$. The dashed line shows the theoretical prediction $\gamma(k) - 3 = 1/[3 \ln(k/k_0)]$ with $k_0 = 1.64k_\xi$.

is the average density and V is the trap volume. The third term implements small-length-scale dissipation. We choose V_{diss} to mimic the dissipation encountered in experiments, *i.e.* evaporative losses when the atom energy exceeds the trap depth U_D [15]. This dissipation term is critical for realizing a steady state in a continuously forced system.

The system is initialized in the ground state of Eq. (1) including $V_{\text{box}}(\mathbf{r})$, which corresponds to a Bose-Einstein condensate with a nearly uniform density, except near the boundary of the box. For relevance, we use numbers typical of recent experiments [13]: the cylindrical box length is $L = 50 \mu\text{m}$ and its radius is $R = 15 \mu\text{m}$, the initial atom number is $N(t=0) = 2 \times 10^5$ and a/a_0 is varied between 25 and 400 (where a_0 is the Bohr radius). The natural energy scale of the system $\zeta \equiv gn(t=0)$ therefore varies between $k_B \times 1.2\text{nK}$ and $k_B \times 19\text{nK}$, the corresponding timescale $\tau \equiv \hbar/\zeta$, between 2.6ms and 42ms, and the natural lengthscale $\xi \equiv \sqrt{2m\zeta}/\hbar$, between $0.6 \mu\text{m}$ and $2.3 \mu\text{m}$ (using the mass m of ^{39}K). The gas is driven at a frequency $\omega/(2\pi)$ that matches the resonance of the lowest-lying Bogoliubov excitation [30]; for our parameters, $\omega/(2\pi)$ ranges from 5 to 20Hz.

As shown in Fig. 1(b), the injection of energy results in a cascade front propagating to higher momenta, until hitting the wavenumber k_D at time $\approx t_D$ [31]. For $t \gtrsim t_D$, the system is in a steady state well described by a power law distribution for the mode occupation number: $N_k \propto k^{-\gamma}$ with $\gamma \approx 3.5$. Here, N_k is the mode occupation number for the states of momentum k , normalized as $\sum_{\mathbf{k}} N_{\mathbf{k}} = N$ (in the language of WWT, N_k is the waveaction spectrum); in the continuous limit, it is related to the momentum distribution $n(k)$ as $N_k = ((2\pi)^3/V)n(k)$.

As the momentum $k_\xi \equiv 1/\xi$ marks the typical momentum scale associated with interactions, we have that for $k \gg k_\xi$, our system is weakly nonlinear, with 4-wave interactions between (bare) particles; our system can then be described by

the theory of WWT [23, 32]. This theory predicts that, in the limit of weak nonlinearities, the momentum distribution of the direct energy cascade has the asymptotic isotropic form $n(k) \propto k^{-3} \ln^{-1/3}(k/k_0)$ where k_0 is the energy injection scale [22]. At lower momenta ($k \lesssim k_\xi$) the particles interact more strongly, and the 4-wave WWT description is not expected to work [33].

However, in any real system, the momentum range over which universal turbulent properties (*i.e.* injection and dissipation independent, boundary condition independent, *etc.*) may exist is finite. Thus, the validity of asymptotic results is questionable, and the observations might depend on the separation between the injection and dissipation scales. To test the dependence of the steady-state $n(k)$ on those scales, we calculate the apparent cascade exponent $\gamma(k) \equiv -d \ln[n(k)]/dk$ for different ξ and k_D . As shown in Fig. 1(c), when γ is plotted versus k for various ξ (but same k_D), it decreases for $k \lesssim k_D/2$ and depends on ξ ; for $k \gtrsim k_D/2$, all $\gamma(k)$ increase together. However, when plotted against $k\xi$, the results are universal in the intermediate regime $2.5 \lesssim k\xi \lesssim k_D\xi/2$; this shows that, despite the fact that the energy is physically injected at the scale $k_F \approx \pi/L$, the effective injection scale for the isotropic 4-wave cascade is actually $k_0 \propto k_\xi (\gg k_F)$ [34]. To test the asymptotic form $n(k) \propto k^{-3} \ln^{-1/3}(k/k_0)$, we fit $\gamma(k)$ with $3 + 1/(3 \ln^{-1/3}[Ak\xi])$ in the regime where the numerical data overlap. We find that for $A = 0.61(1)$, the fit captures the data well. Equivalently, this fit predicts that the injection scale for the isotropic 4-wave cascade is $k_0 = 1.64(2)k_\xi$ (as long as $k_F \ll k_\xi$ [35]). The convergence towards a robust steady state, *i.e.* that is independent of ξ , ω , k_D , and U_s , and that matches a universal expectation that is independent of both the driving protocol and the macroscopic nature of the dissipation, strongly suggests that we have access here to intrinsic properties of the universal GP model Eq. (1).

As was already presumed experimentally [13, 14], we find

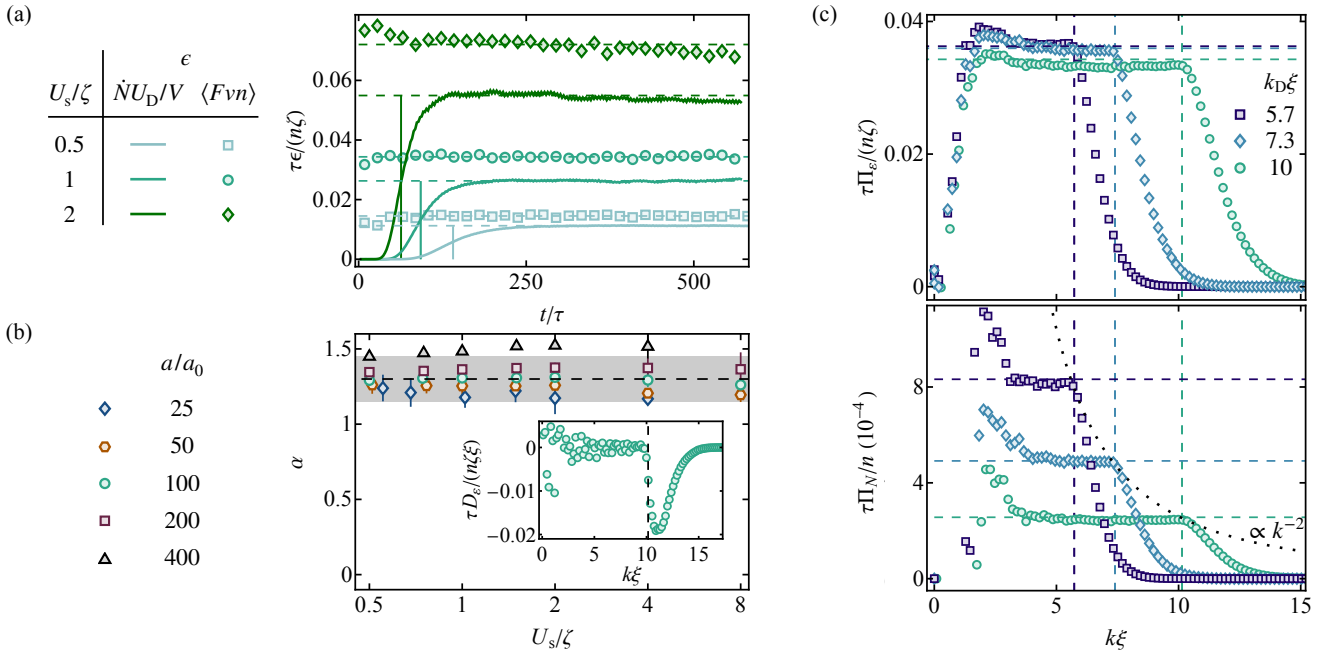


FIG. 2. Energetics of the direct turbulent cascade. (a) Energy input and dissipation rates. We show $\tau\epsilon/(n\zeta)$ where ϵ is either the energy injection rate calculated as $\epsilon_{in} \equiv \langle Fvn \rangle$ (symbols) or the particle dissipation rate \dot{N} multiplied by U_D/V (solid lines). Both ϵ_{in}/n and $\dot{N}U_D/V$ are constant at long times (see also [27]), but ϵ_{in}/n is higher by a factor of ≈ 1.3 . The vertical solid lines mark the onset time of dissipation t_D ; for an analytical calculation of t_D , see [27]. (b) The ratio α of ϵ_{in} and $\dot{N}U_D/V$ for different drive strengths U_s/ζ and scattering lengths a/a_0 . Inset: the dissipation spectrum D_ϵ for $U_s = \zeta$ and $a = 100a_0$. The average dissipation momentum $\langle k_{diss} \rangle \approx 1.15k_D$, predicting $\alpha \approx 1.32$ (see text). (c) Energy flux Π_ϵ (top) and particle flux Π_N (bottom) for different dissipation scales k_D (vertical dashed lines). Both fluxes are scale independent. The dotted line ($\propto k^{-2}$) shows that $\Pi_N \propto k_D^{-2}$, while Π_ϵ is (nearly) independent of k_D ; horizontal dashed lines are ϵ_{in} (resp. $\tau\dot{N}/N$) in the upper (resp. lower) panel (see text).

that a power law $n(k) \propto k^{-\gamma_0}$ with an effective exponent $\gamma_0 = 3.5$ accurately captures all the relevant details, since the variation of the logarithmic correction for $\gamma(k)$ is small over the relevant momentum range (see also a discussion in [27]). From now on, we fix $n(k)$ to this power law and define the amplitude of the power law $n_0 \equiv N_k k^3 (k\xi)^{\gamma_0-3}$.

We next turn to the calculation of the energy-density input and dissipation rates. As energy is injected into the system by the forcing potential $V_{drive}(\mathbf{r}, t) = U_s \sin(\omega t) z/L$, the energy input rate can be calculated as $\epsilon_{in} \equiv \langle Fvn \rangle$ where $F \equiv -\hat{z} \cdot \nabla V_{drive}$ (where \hat{z} is the unit vector along z), v is the center-of-mass velocity of the gas and the averaging is performed over a drive period. The energy is dissipated at high momenta solely by particles with momenta $k > k_D$ leaving the trap. Hence, in previous experimental works [13, 15], the energy dissipation rate was determined as $\dot{N}U_D$ where \dot{N} is the particle loss rate. However, as shown in Fig. 2(a) for three different U_s , the energy-density injection rate ϵ_{in} is consistently higher than $\dot{N}U_D/V$. While $\dot{N}U_D/V$ is initially zero and increases smoothly to its final value when the system approaches the steady state, this final value is always lower than ϵ_{in} . We investigate this discrepancy systematically by showing the ratio $\alpha = V\epsilon_{in}/(\dot{N}U_D)$ for different U_s and a in Fig. 2(b). The ratio $\alpha \approx 1.3$ is independent of U_s [36]. The reason for $\alpha \neq 1$ is the shape of the dissipation spectrum $D_\epsilon(k)$ (see [27] for a

formal definition): calculating the energy-density dissipation rate as $\dot{N}U_D/V$ assumes that the dissipation happens exactly at energy U_D . As shown in the inset of Fig. 2(b) for a typical $U_s = \zeta$ and $a = 100a_0$, $D_\epsilon(k)$ has a sharp onset at k_D , but has a significant tail above k_D . The average dissipation momentum is $\langle k_{diss} \rangle \equiv \int k D_\epsilon(k) dk / \int D_\epsilon(k) dk \approx 1.15k_D$, showing that the energy dissipated from the system per unit time is $\approx 1.32\dot{N}U_D$.

Having verified that the energy input (at low k) and dissipation (at high k) rates are equal, we turn to the direct calculation of the scale-resolved energy flux $\Pi_\epsilon(k)$ and particle flux $\Pi_N(k)$ (see [27] for the formal definition of the fluxes). As shown in Fig. 2(c), Π_ϵ is momentum independent in steady state and equal to the energy injection rate ϵ_{in} . The energy injected at low k is transported to higher k by the momentum-independent flux $\Pi_\epsilon(k)$ and dissipated at $\gtrsim k_D$. As expected for an energy cascade, Π_ϵ is also (nearly) independent of the dissipation scale k_D [37]. On the other hand, Π_N is also momentum independent in steady state, but its plateau value decreases as $\propto k_D^{-2}$, as expected for particles with a quadratic dispersion relation [see dotted line in the lower panel of Fig. 2(c)] [38]. We define ϵ , the scale-invariant energy-density flux, as the plateau value of Π_ϵ ; in the rest of the paper we compute ϵ as $\langle Fvn \rangle$.

Finally, we investigate the relation between the two far-from-equilibrium state variables of the system, ϵ and n_0 .

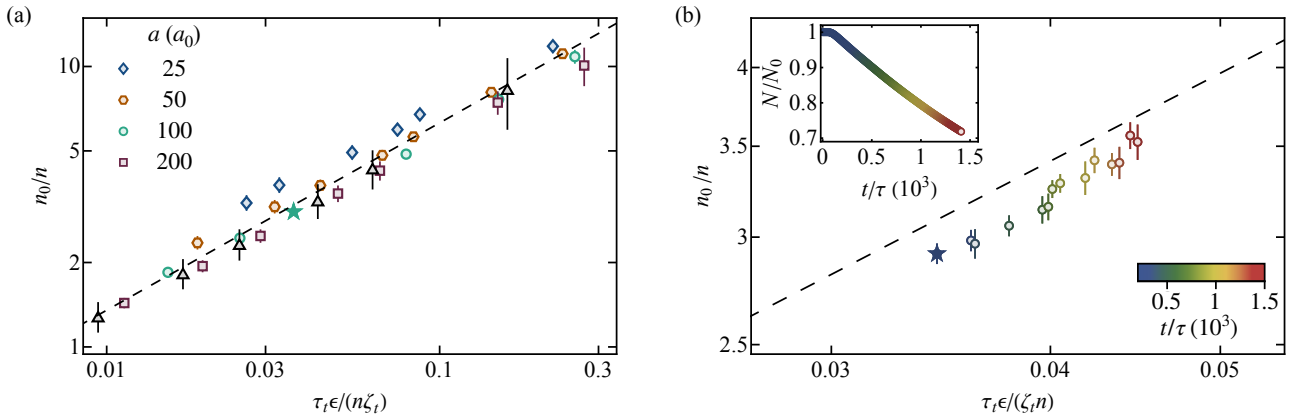


FIG. 3. (a) A universal equation of state of the GP model. Expressing the state variables ϵ and n_0 in the instantaneous natural scales of the GP model (n , ξ_t , ζ_t , τ_t) collapses data at different a onto a universal curve. The dashed line is a power-law fit to the data that gives $n_0/n = 29(2)(\tau_t \epsilon / [n \zeta_t])^{0.67(2)}$. (b) The instantaneous far-from-equilibrium state variables for different t follow the EoS, in analogy with an equilibrium-thermodynamics quasi-static process; the data correspond to $a = 100a_0$, see the green star in panel (a). The points in panel (a) correspond to shaking times $\approx 2t_D$ and the green star in (a) is the same point as the blue star in (b). The inset shows the fraction of particles N/N_0 left in the system.

Fig. 3(a) shows n_0 and ϵ for different a ; we express both state variables using the instantaneous natural scales of the GP equation ξ_t , τ_t , and ζ_t defined through the instantaneous density n [39]. Data for different values of a fall on a (nearly) universal curve, demonstrating that the only relevant scales describing the turbulent cascade are the intrinsic scales of the universal GP model Eq. (1) and all the dependence on the system and drive scales (L , R , U_s , ω , k_D) drops out [40].

We find that the GP model contains a turbulent EoS that is a power law of the form $n_0/n = C(\tau_t \epsilon / [n \zeta_t])^b$, with $C = 29(2)$ and $b = 0.67(2)$, which is not described by known paradigms of turbulence. In particular, it cannot be explained by 4-wave processes: the relation between n_0 and ϵ would have to be independent of the total density n which is not the case for the EoS constructed here [41]. Furthermore, the power-law exponent $0.67(2)$ is inconsistent with any wave-kinetic description, as a kinetic theory with ℓ -wave interactions predicts an exponent $b = 1/(\ell - 1) \leq 0.5$. Interestingly, this exponent for the amplitude of mode occupation is numerically the same as the exponent for the amplitude of the energy spectrum for hydrodynamic turbulence $E_{K41} \propto \epsilon^{2/3}$ [42]. However, this is likely coincidental. First, these quantities are different; one step further: the energy spectrum associated with our N_k is $E(k) \propto k^{0.5}$ for $\gamma = 3.5$ (assuming a quadratic dispersion relation), while $E_{K41} \propto k^{-5/3}$. Secondly, the predictions of K41 are independent of interactions, while our universal EoS strongly depends on them (as the rescaling of ϵ with ζ_t/τ_t corresponds to a rescaling with a^2).

Finally, we note that the slow decrease of N due to evaporative losses above k_D implements a slow thermodynamic-like process. Indeed, as N decreases, the state variable $\epsilon \propto N$ also decreases, resulting in a slow change of the far-from-equilibrium state (see also [27]). In Fig. 3(b), we show that the simultaneous change of the state variables ϵ and n_0 follows the EoS: when rescaled to the instantaneous GP scales,

the instantaneous ϵ and n_0 ‘slide up’ on our universal EoS line over time, see blue to red shades [43]. This is reminiscent of the concept of thermodynamic quasi-static processes, for which infinitesimal changes of external constraints take a system through a dense succession of equilibrium states [44]. Remarkably, we find that this concept generalizes to states that are even locally far from equilibrium.

In conclusion, we numerically investigated the properties of a turbulent cascade arising in the GP model when a box trapped gas is periodically driven and showed that it can be described by a universal EoS relating the turbulent state variables, the energy flux and the cascade amplitude. The form of our EoS is inconsistent with any kinetic theory, posing a new theoretical challenge. The comparison of our mean-field simulations to experimental measurements provides valuable benchmarks for testing the validity of mean-field theories in far-from-equilibrium scenarios. Note that even though our work provides some elements to understand the experimental results of [13], the experimental EoS cannot be fully understood solely within the framework of the GP model as the data features a scaling with na^3 that is incompatible with the universal GP model (see also [27]). In the future, it would be interesting to study on its own the incompressible parts of this turbulent scenario [19]. One should also investigate the fluctuations of N_k ; comparing these fluctuations between experiments and classical field simulations could shed light on the role of quantum fluctuations in turbulent quantum fluids.

We thank M. Gazo, J. Etrych, C. Eigen, G. Krstulovic, M. Tsubota, G. Falkovich, and V. L’vov for discussions. This work was supported by the NSF (Grant Nos. PHY-1945324 and PHY-2110303), DARPA (Grant No. HR00112320038), the David and Lucile Packard Foundation, the Alfred P. Sloan Foundation, and JSPS KAKENHI (Grant No. JP23K13029). G.M. acknowledges support from Trinity College (Cambridge) and Yale University for its hospitality.

* gm572@cam.ac.uk

- [1] P. C. Hohenberg and B. I. Halperin, Theory of dynamic critical phenomena, *Rev. Mod. Phys.* **49**, 435 (1977).
- [2] A. J. Bray, Theory of phase-ordering kinetics, *Advances in Physics* **43**, 357 (1994).
- [3] D. Forster, *Hydrodynamic fluctuations, broken symmetry, and correlation functions* (CRC Press, 2018).
- [4] J. Berges, A. Rothkopf, and J. Schmidt, Nonthermal Fixed Points: Effective Weak Coupling for Strongly Correlated Systems Far from Equilibrium, *Phys. Rev. Lett.* **101**, 041603 (2008).
- [5] S. Erne, R. Bückler, T. Gasenzer, J. Berges, and J. Schmiedmayer, Universal dynamics in an isolated one-dimensional Bose gas far from equilibrium, *Nature* **563**, 225 (2018).
- [6] M. Prüfer, P. Kunkel, H. Strobel, S. Lannig, D. Linnemann, C.-M. Schmied, J. Berges, T. Gasenzer, and M. K. Oberthaler, Observation of universal dynamics in a spinor Bose gas far from equilibrium, *Nature* **563**, 217 (2018).
- [7] J. A. P. Glidden, C. Eigen, L. H. Dogra, T. A. Hilker, R. P. Smith, and Z. Hadzibabic, Bidirectional dynamic scaling in an isolated Bose gas far from equilibrium, *Nat. Phys.* **17**, 457 (2021).
- [8] M. Gałka, P. Christodoulou, M. Gazo, A. Karailiev, N. Dogra, J. Schmitt, and Z. Hadzibabic, Emergence of Isotropy and Dynamic Scaling in 2D Wave Turbulence in a Homogeneous Bose Gas, *Phys. Rev. Lett.* **129**, 190402 (2022).
- [9] M. Gazo, A. Karailiev, T. Satoor, C. Eigen, M. Gałka, and Z. Hadzibabic, Universal Coarsening in a Homogeneous Two-Dimensional Bose Gas, arXiv:2312.09248 (2023).
- [10] S. Huh, K. Mukherjee, K. Kwon, J. Seo, J. Hur, S. I. Mistakidis, H. R. Sadeghpour, and J.-y. Choi, Universality class of a spinor Bose-Einstein condensate far from equilibrium, *Nat. Phys.* **20**, 402 (2024).
- [11] S. C. Takatori and J. F. Brady, Towards a thermodynamics of active matter, *Phys. Rev. E* **91**, 032117 (2015).
- [12] F. Ginot, I. Theurkauff, D. Levis, C. Ybert, L. Bocquet, L. Berthier, and C. Cottin-Bizonne, Nonequilibrium Equation of State in Suspensions of Active Colloids, *Phys. Rev. X* **5**, 011004 (2015).
- [13] L. H. Dogra, G. Martirosyan, T. A. Hilker, J. A. P. Glidden, J. Etrych, A. Cao, C. Eigen, R. P. Smith, and Z. Hadzibabic, Universal equation of state for wave turbulence in a quantum gas, *Nature* **620**, 521 (2023).
- [14] N. Navon, A. L. Gaunt, R. P. Smith, and Z. Hadzibabic, Emergence of a turbulent cascade in a quantum gas, *Nature* **539**, 72 (2016).
- [15] N. Navon, C. Eigen, J. Zhang, R. Lopes, A. L. Gaunt, K. Fujimoto, M. Tsubota, R. P. Smith, and Z. Hadzibabic, Synthetic dissipation and cascade fluxes in a turbulent quantum gas, *Science* **366**, 382 (2019).
- [16] G. Fibich, *The nonlinear Schrödinger equation*, Vol. 192 (Springer, 2015).
- [17] L. Pitaevskii and S. Stringari, *Bose-Einstein condensation and superfluidity* (Oxford University Press, Oxford, 2016).
- [18] There also exists a vast body of work on the topic of vortex turbulence in the GP model (see e.g. [19] and references therein).
- [19] M. Kobayashi, P. Parnaudeau, F. Luddens, C. Lothodé, L. Danaïla, M. Brachet, and I. Danaïla, Quantum turbulence simulations using the gross-pitaevskii equation: high-performance computing and new numerical benchmarks, *Computer Physics Communications* **258**, 107579 (2021).
- [20] S. Dyachenko, A. Newell, A. Pushkarev, and V. Zakharov, Optical turbulence: weak turbulence, condensates and collapsing filaments in the nonlinear schrödinger equation, *Physica D* **57**, 96 (1992).
- [21] G. Falkovich and I. Ryzhenkova, Kolmogorov spectra of langmuir and optical turbulence, *Physics of Fluids B: Plasma Physics* **4**, 594 (1992).
- [22] Y. Zhu, B. Semisalov, G. Krstulovic, and S. Nazarenko, Direct and inverse cascades in turbulent bose-einstein condensates, *Phys. Rev. Lett.* **130**, 133001 (2023).
- [23] V. E. Zakharov, V. S. L'Vov, and G. Falkovich, *Kolmogorov spectra of turbulence* (Springer Berlin, 1992).
- [24] G. P. Agrawal, Nonlinear fiber optics, in *Nonlinear Science at the Dawn of the 21st Century* (Springer, 2000) pp. 195–211.
- [25] P. G. Kevrekidis, D. J. Frantzeskakis, and R. Carretero-González, *Emergent nonlinear phenomena in Bose-Einstein condensates: theory and experiment*, Vol. 45 (Springer, 2008).
- [26] W. Craig, C. Sulem, and P.-L. Sulem, Nonlinear modulation of gravity waves: a rigorous approach, *Nonlinearity* **5**, 497 (1992).
- [27] Supplemental Material.
- [28] N. Navon, R. P. Smith, and Z. Hadzibabic, Quantum gases in optical boxes, *Nat. Phys.* **17**, 1334 (2021).
- [29] Note that even though the trap shape affects large-scale properties, the far-from-equilibrium state at smaller scales is largely insensitive to the details of the confining potential.
- [30] S. J. Garratt, C. Eigen, J. Zhang, P. Turzák, R. Lopes, R. P. Smith, Z. Hadzibabic, and N. Navon, From single-particle excitations to sound waves in a box-trapped atomic bose-einstein condensate, *Phys. Rev. A* **99**, 021601 (2019).
- [31] In [27], we derive an analytic expression for t_D in terms of the cascade properties.
- [32] S. Nazarenko, *Wave turbulence* (Springer, 2011).
- [33] In the presence of a condensate, the proper quasiparticles to consider for $k\xi \lesssim 1$ are the Bogoliubov phonons, for which the appropriate WWT description is a wave-kinetic equation with 3-wave interactions. In our simulations, a description in terms of an equilibrium-like condensate is meaningless since for our strong drives, the Bogoliubov approximation is invalid.
- [34] Interestingly, a recent experiment has observed that the momentum distribution of 2D shaken Bose gases also becomes isotropic at $k \approx k_\xi$ [8].
- [35] Experimentally, k_D is bounded, so the separation between the injection scale $k_0 \propto k_\xi$ and k_D – and hence the region where the 4-wave WWT theory is applicable – is reduced for stronger interactions.
- [36] Even though $\alpha \neq 1$ means that the energy-density flux is not $\dot{N}U_D/V$, the fact that α has only a very weak dependence on a ($\propto a^{0.08(1)}$) and is independent of U_ξ suggests that the determination of the energy flux via $\dot{N}U_D/V$, as done in [13, 15], will only introduce a small, presumably system-specific, systematic error.
- [37] Note that the slow decrease of the plateau of Π_ϵ is due to a progressive depletion of the condensate, which results in a (slow) decrease of ϵ_{in} [corresponding horizontal dashed lines in the upper panel of Fig. 2(c)].
- [38] Note that it is only in the limit $k_D \rightarrow \infty$ that one recovers the expected limits $\Pi_\epsilon \rightarrow \epsilon$ with $\Pi_N \rightarrow 0$ for the direct energy cascade [20].
- [39] Note that ξ_t is not directly present in the axes of Fig. 3, but is used in the calculation of $n_0 = N_k k^{-3} (k\xi_t)^{-0.5}$.
- [40] The independence of our EoS with k_D cannot rigorously hold as for large enough k_D (presumably beyond what we explored), WWT results should be recovered.
- [41] The factor of $\xi^{0.5}$ on the y-axis is a finite- k_D effect, but even in

its absence our EoS would depend on n ; within the GP model, only the WWT prediction of a power-law EoS with an exponent of 1/3 is independent of n .

[42] U. Frisch, *Turbulence: the legacy of A.N. Kolmogorov* (Cambridge University Press, 1995).

[43] As shown in [27], n_0 and ϵ/n are roughly constant over time,

resulting in the increase of n_0/n and $\tau_\epsilon/(n\zeta_\epsilon)$.

[44] H. B. Callen, *Thermodynamics and an Introduction to Thermostatistics* (John Wiley & Sons, 1991).

[45] We benchmarked our simulations for different choices of A and w and have verified their choice within an appropriate range does not affect our results.

SUPPLEMENTAL MATERIAL

I. SIMULATION DETAILS

Our numerical simulations solve the time-dependent GP equation [Eq. (1)] using a pseudo-spectral method with the fourth-order Runge-Kutta time evolution. We add potential terms to the GP equation to implement the box trapping and to provide energy injection (which conserves particle number) and dissipation (which does not):

$$i\hbar\frac{\partial\psi}{\partial t} = \left(-\frac{\hbar^2}{2m}\nabla^2 + g|\psi|^2 + V_{\text{box}}(\mathbf{r}, t) + V_{\text{drive}}(\mathbf{r}, t) + V_{\text{diss}}(\mathbf{r}, t)\right)\psi. \quad (\text{S1})$$

These potentials are selected for their experimental relevance [13, 15]. The cylindrical box potential, whose depth is U_D and symmetry axis is along z , is:

$$V_{\text{box}}(\mathbf{r}, t) = \begin{cases} 0, & \text{if } |z| < L/2 \text{ and } x^2 + y^2 < R^2 \\ U_D, & \text{otherwise,} \end{cases}$$

V_{drive} is the time-periodic potential gradient:

$$V_{\text{drive}}(\mathbf{r}, t) = \frac{U_s}{L} \sin(\omega t) z,$$

and V_{diss} is an absorbing potential on the edges of the simulation grid to mimic the loss of particles that have enough energy to leave the box:

$$V_{\text{diss}} = -iA \text{Max} \left[\cosh^2 \left(\frac{1}{w} [1 - |x|/D_x] \right), \cosh^2 \left(\frac{1}{w} [1 - |y|/D_y] \right), \cosh^2 \left(\frac{1}{w} [1 - |z|/D_z] \right) \right];$$

here D_σ is the simulation grid size along direction σ , A and w are the strength and the characteristic width of the absorbing boundary [45].

Our simulations are typically performed on a grid of size $128 \times 128 \times 256$ (for the data at the highest k_D in Fig. 1(c), we use a $256 \times 256 \times 512$ grid to ensure that the highest accessible momenta in the simulations are $> k_D$). Our temporal resolution is $\approx 0.1\hbar/U_D$.

II. CALCULATING MOMENTUM-RESOLVED FLUXES

The equation of motion for the energy-density spectrum, $\epsilon(k, t) = 1/n \int_{|\mathbf{k}'|=k} n(\mathbf{k}') \hbar^2 |\mathbf{k}'|^2 / (2m) d\mathbf{k}'$ (where the time dependence of $n(\mathbf{k}')$ is omitted for convenience) is obtained directly from the GP equation by taking the time derivative of $\epsilon(k, t)$:

$$\frac{\partial}{\partial t} \epsilon(k, t) + \frac{\partial}{\partial k} \Pi_\epsilon(k, t) = F_\epsilon(k, t) + D_\epsilon(k, t). \quad (\text{S2})$$

The energy-density flux Π_ϵ is

$$\Pi_\epsilon(k, t) = \frac{1}{i\hbar} \int_k^\infty dk_1 \int_{|\mathbf{k}'|=k_1} \frac{\hbar^2 |\mathbf{k}'|^2}{2m} (\tilde{\psi}^*(\mathbf{k}') \mathbb{FT} [g|\psi|^2 \psi](\mathbf{k}') - \text{c.c.}) d\mathbf{k}',$$

where $\tilde{\psi}(\mathbf{k})$ is the Fourier transform of $\psi(\mathbf{r})$ (the time dependence of $\tilde{\psi}$ and ψ are omitted for convenience), \mathbb{FT} denotes the Fourier transform, and c.c. denotes the complex conjugate. The terms F_ϵ and D_ϵ are the (system-dependent) forcing and dissipation terms respectively:

$$F_\epsilon(k, t) = \frac{1}{i\hbar} \int_{|\mathbf{k}'|=k} \frac{\hbar^2 |\mathbf{k}'|^2}{2m} \left(\tilde{\psi}^*(\mathbf{k}') \mathbb{FT} \left[\frac{U_s}{L} z \sin(\omega t) \psi \right](\mathbf{k}') - \text{c.c.} \right) d\mathbf{k}',$$

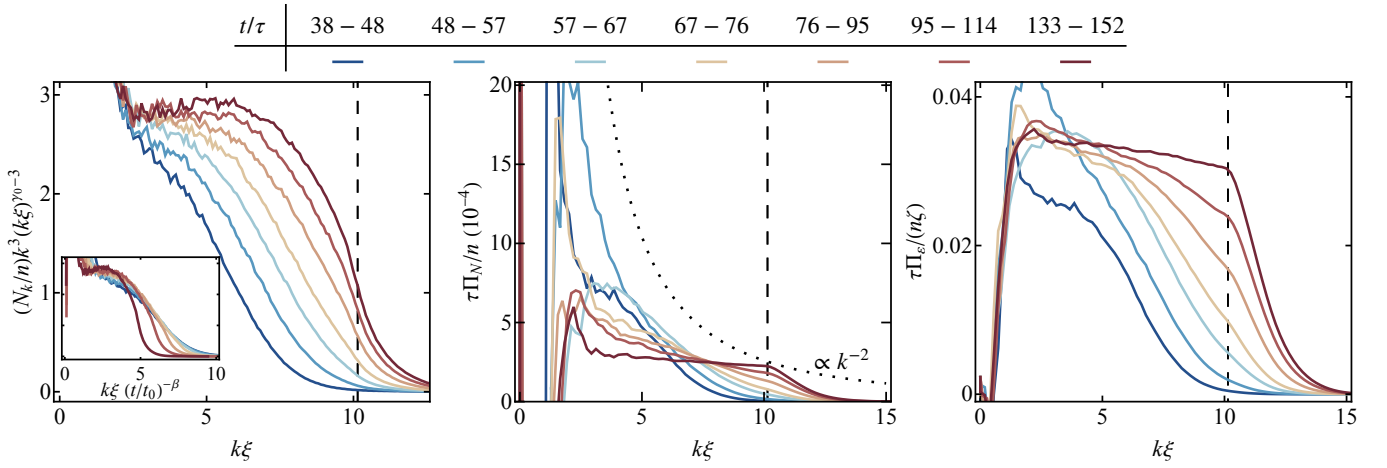


FIG. S1. Sharpness of the cascade front. The compensated spectrum $\propto N_k k^{\gamma_0}$ (left), the particle flux $\Pi_N(k)$ (middle), and the energy flux $\Pi_\epsilon(k)$ (right) for various times. During the cascade buildup, neither the spectrum nor the fluxes have sharp fronts. The dissipation scale k_D acts as a sharp cutoff in momentum space and results in a sharp drop-off of the fluxes above k_D . The inset on the left panel shows the compensated spectrum with the x -axis rescaled by $(t/t_0)^{-\beta}$ showing that the cascade propagation is only approximately dynamically scalable; here $\beta = 2/3$ is calculated from $\gamma_0 = 3.5$, and $t_0 = 0.5$ s is an arbitrary reference time. The dotted line in the middle plot is a reference $\propto k^{-2}$, same as in Fig. 2(c).

and

$$D_\epsilon(k, t) = \frac{1}{i\hbar} \int_{|\mathbf{k}'|=k} \frac{\hbar^2 |\mathbf{k}'|^2}{2m} (\tilde{\psi}^*(\mathbf{k}') \text{FT}[V_{\text{box}}\psi + V_{\text{abs}}\psi](\mathbf{k}') - \text{c.c.}) d\mathbf{k}'.$$

The analog of Eq. (S2) for the particle density spectrum $1/n \int_{|\mathbf{k}'|=k} n(\mathbf{k}') d\mathbf{k}'$ is derived along similar lines, and the corresponding particle-density flux Π_N is

$$\Pi_N(k, t) = \frac{1}{i\hbar} \int_k^\infty dk_1 \int_{|\mathbf{k}'|=k_1} (\tilde{\psi}^*(\mathbf{k}') \text{FT}[g|\psi|^2\psi](\mathbf{k}') - \text{c.c.}) d\mathbf{k}'.$$

The results presented in Fig. 2(b)-(c) are obtained by direct calculations of the above formulae.

III. SHARPNESS OF THE CASCADE FRONT

In WWT theory, the interactions between waves are usually assumed to be local in momentum space, *i.e.* interactions are significant only between waves of nearby momenta, resulting in a sharp cascade front propagating in momentum space. This locality arises from the conservation of energy and momentum: the most likely interactions satisfying those conservation laws are the ones that result in a small change of momenta. The effects of the conservation laws depend on the dimensionality and are more pronounced in lower dimensions. It turns out that WWT predicts that the direct energy cascade in the 3D GP model is not strictly local due to a weak (logarithmic) divergence at low k [20–22]. In Fig. S1 we show that both the compensated spectrum $(N_k/n)k^3(k\xi)^{\gamma_0-3}$ and the energy flux Π_ϵ do not have sharp edges before hitting k_D . Because of this, the energy dissipation rate $\dot{N}U_D$ grows smoothly from 0 to its final value rather than sharply jumping at t_D (see Fig. 2(a)). However, once the dissipation scale k_D is reached, it enforces a sharp cutoff to the flux, resulting in the textbook behavior versus k_D shown in Fig. 2(c).

IV. THE ONSET TIME FOR DISSIPATION

Here we calculate the time t_D when the system starts to dissipate energy. As shown in Fig. S1, the cascade front is not sharp, so the onset of dissipation is not very sharp either. To define t_D , we fit the fractional particle loss \dot{N}/N with a piece-wise linear function and identify t_D as the singular point of the piece-wise function [Fig. S2(a)]. In Fig. S2(b), we show t_D versus ϵ for different a ; t_D monotonically decreases with ϵ for a given interaction strength but the relation is not single valued for different a .

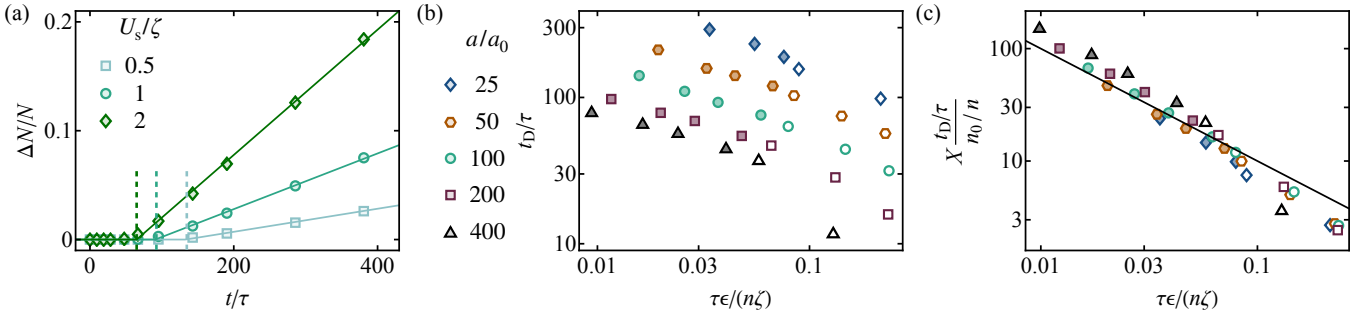


FIG. S2. The onset time for dissipation. (a) Number of particles lost from the system ΔN for different drive strengths U_s/ζ ; here $a = 100a_0$. The lines are piece-wise linear fits, indicating that dissipation begins after a cascade build-up time t_D (vertical colored dashed lines). (b,c) Onset time for dissipation t_D as a function of ϵ . (b) The relation is monotonic for a given interaction strength, but the data for t_D at different interaction strengths are not universal. (c) The onset times can be analytically calculated assuming that ϵ is constant over time [for the explicit expression of X , see Eq. (S3)]. The solid black line is the theoretical expectation $n\zeta/(\tau\epsilon)$. The closed (resp. open) symbols correspond to driving with $U_s \leq 1.5\zeta$ (resp. $U_s > 1.5\zeta$). For $U_s \leq 1.5\zeta$, the energy input rate is constant in time to within 10%.

Remarkably, t_D can be calculated analytically under the assumption that the energy input rate is constant and that the onset of dissipation is sharp at $k = k_D$. As the momentum distribution has the form $n(k) = V/(2\pi)^3 n_0 k^{-3} (k\xi)^{-\gamma_0+3}$, the total energy of the system in the steady state is

$$\int_0^{k_D} 4\pi k^2 n(k) \frac{\hbar^2 k^2}{2m} dk = n_0 \frac{U_D V (k_D \xi)^{3-\gamma_0}}{2\pi^2 (5-\gamma_0)}.$$

Equating this to the energy injected into the system up until t_D yields

$$\frac{t_D}{\tau} = \frac{U_D (k_D \xi)^{3-\gamma_0}}{2\pi^2 (5-\gamma_0) \zeta} \frac{n_0/n}{\tau \epsilon / n \zeta} \equiv X \frac{n_0/n}{\tau \epsilon / n \zeta}. \quad (\text{S3})$$

In Fig. S2(c) we show that t_D is in excellent agreement with this calculation for weak drives ($U_s \leq 1.5\zeta$), while for stronger drives the constant- ϵ assumption fails and t_D is shorter [open symbols in Fig. S2(c)].

We note that despite the weak nonlocality discussed in section III, the dissipation onset time t_D matches the analytical prediction. In Fig. 2(a), we see that the curves for $\dot{N}U_D/N$ are slightly rounded before reaching their steady-state value but t_D is an approximate point of symmetry where the (unaccounted) energy dissipation before t_D matches the not-yet-fully-saturated dissipation after t_D .

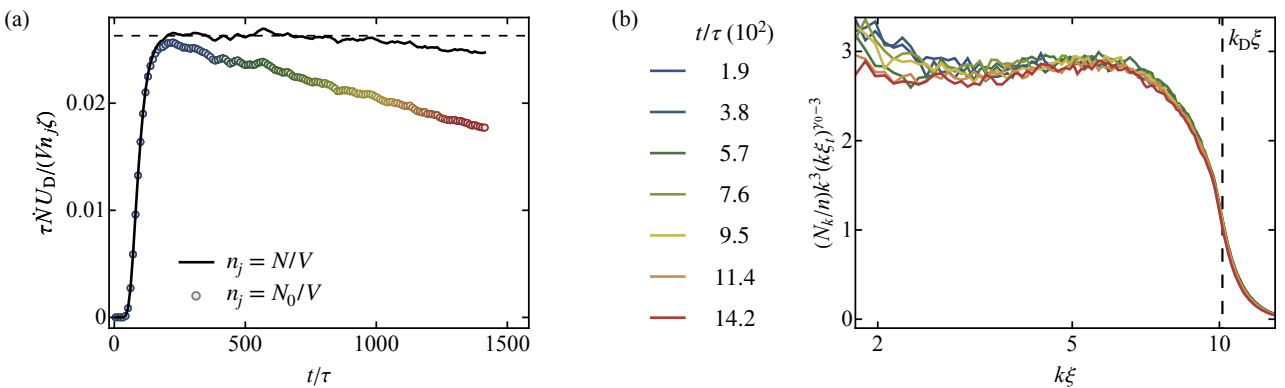


FIG. S3. Time dependence of state variables. (a) The particle-density dissipation rate \dot{N}/V multiplied by U_D and normalized to n_j . As a black solid line (resp. colored symbols), we show $\dot{N}U_D/V$ normalized to $n_j = N/V$ (resp. $n_j = N_0/V$), the instantaneous density (resp. initial density). After the steady state is fully established, the former is constant while the latter decreases as atoms leave the trap. (b) The compensated spectrum $(N_k/n)k^3(k\xi_t)^{\gamma_0-3}$ is constant over time, even though the energy flux has significantly decreased. The color coding is the same in the two panels.

V. TIME DEPENDENCE OF THE STATE VARIABLES

For long drive times, the atom loss becomes significant, resulting in a depletion of the low- k population and thus a decrease in the total energy injection rate into the system [$\propto N$, Fig. S3(a)]. On the other hand, the compensated spectrum $N_k k^3 (k\xi_t)^{\gamma_0-3}$ is constant (Fig. S3(b)). This can be understood from the shape of the EoS as follows: ϵ decreases as $1/N$, but $\tau_t/(n\xi_t)$ increases as N^3 , resulting in n_0/n increasing as $N^{4/3}$ (assuming that the EoS is $n_0 \propto \epsilon^{2/3}$). This means that $(N_k/n)k^3(k\xi_t)^{\gamma_0-3}$ increases as $N^{13/12}$ for $\gamma_0 = 3.5$, and therefore the compensated spectrum $N_k k^3 (k\xi_t)^{\gamma_0-3}$ increases as $N^{1/12}$, too weak to be observed.

VI. COMPARISON OF OUR NUMERICAL EoS WITH THE PREDICTION OF WWT THEORY

In the main text, we define the cascade amplitude as $n_0 = N_k k^3 (k\xi)^{\gamma_0-3}$; however, as shown in Fig. 1(c), N_k is not exactly a power law and therefore the cascade amplitude should be more rigorously defined as $n_0^{\text{ln}} \propto N_k k^3 \ln(k/k_0)^{1/3}$. Using the results of Fig. 1(c), we define $n_0^{\text{ln}} = 2N_k k^3 \ln(k/k_0)^{1/3}$ with $k_0 = 1.64k_\xi$ (see Fig. 1). In Fig. S4 we show n_0 (as gray symbols) and n_0^{ln} (as colored symbols), together with power-law fits to both. The two amplitudes are nearly identical, and the power-law fits give EoS exponents of 0.67(2) and 0.60(2) for n_0 and n_0^{ln} , so that the conclusions in the main text are unaffected (note that the factor of 2 in the definition of n_0^{ln} was chosen so that the amplitudes defined from the power law and with the \ln correction are numerically close for our range of parameters; however, their respective dependence on ϵ is independent of that choice).

Additionally, we show in Fig. S4 the n_0^{ln} corresponding to the analytical prediction of the 4-wave WWT cascade $N_k/n = (2\pi)^{8/3} C_d (\tau\epsilon/n\xi)^{1/3} k^{-3} \ln[k/k_0]^{1/3}$ where $C_d \approx 0.0526$ [22] and $k_0 = 1.64k_\xi$ (dash-dotted red line). The WWT predictions are similar to our observations, but the EoS exponent is clearly distinct.

VII. COMPARISON OF OUR NUMERICAL EoS WITH THE EXPERIMENTAL MEASUREMENTS

In Fig. S5 we compare our calculations with the experimental measurements [13]. As the cascade exponent γ_0 used to define n_0 is different in the two cases ($\gamma_0 = 3.5$ for our simulations and $\gamma_0 = 3.2$ in [13]), the comparison of n_0 depends (weakly) on k . To convert n_0 reported in [13] to our definition with $\gamma_0 = 3.5$, we use k in the middle of the experimental cascade range and use k at the edges of the range to assess the uncertainty of the experimental data due to this correction; we use this uncertainty as an error bar for experimental points. We also multiply the experimentally measured fluxes by $\alpha = 1.3$ to account for the difference between ϵ and $\dot{N}U_D/V$. In Fig. S5, the experimental data [13] is displayed as colored symbols, and our numerical results as gray symbols. The experimental data lie systematically above the numerical results. As already noted in [13], the rescaling of the universal EoS with na^3 is incompatible with the universal GP model. However, we note that in the limit $n \rightarrow \infty$ and $na^3 \rightarrow 0$ the GP model is expected to be a good description of the experimental setting and Fig. S5 shows that the experimental data appear to approach our numerical results for lower na^3 .

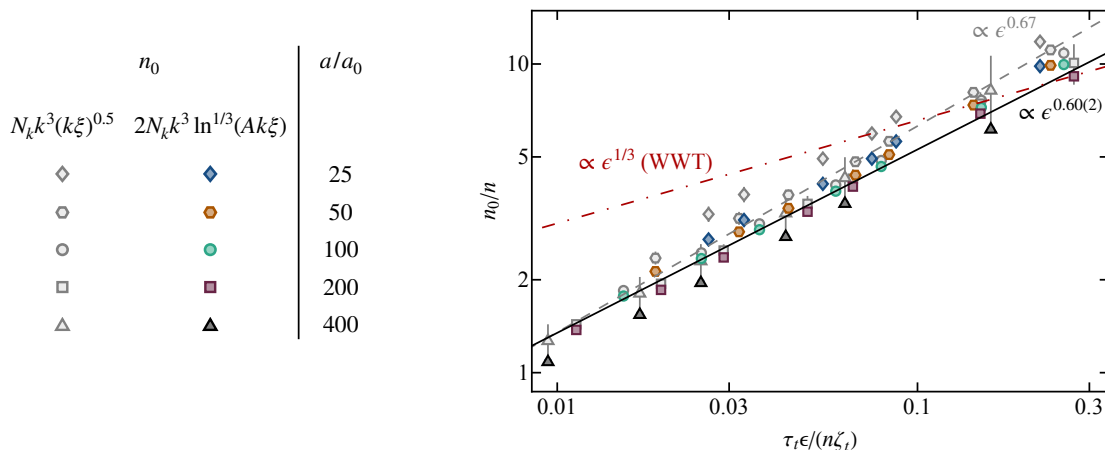


FIG. S4. Comparison of our numerical EoS with the predictions of WWT theory. For the gray symbols (same as in Fig. 3) the cascade amplitude n_0 is defined as $n_0 = N_k k^3 (k\xi)^{0.5}$ while for colored symbols as $n_0 = 2N_k k^3 \ln^{1/3}(Ak\xi)$ with $A = 0.61$. The black solid (resp. gray dashed) lines are power-law fits to the colored (resp. gray) symbols, giving a power law exponent 0.60(2) [resp. 0.67(2)]. The red dash-dotted line shows the prediction of WWT theory for the 4-wave direct cascade without any adjustable parameters.

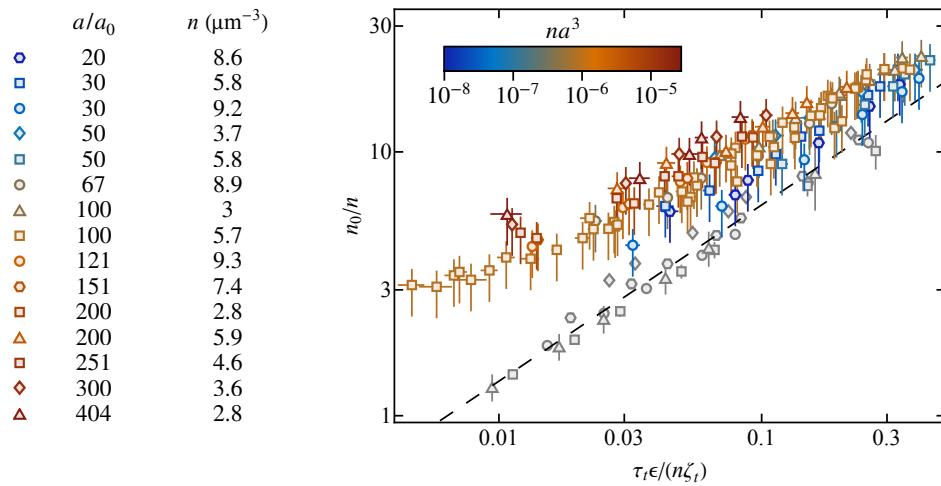


FIG. S5. The comparison of our numerical EoS (gray symbols) with the experimental data [13] (colored symbols). The color coding of the experimental data corresponds to the gas parameter na^3 , and the experimental fluxes are multiplied by 1.3 compared to the data of [13] to account for $\alpha \neq 1$. The vertical error bars of the experimental data represent the uncertainties due to different γ_0 in simulations and experiments.